Gondwana Research 136 (2024) 84–91

Contents lists available at ScienceDirect

Gondwana Research

journal homepage: www.elsevier.com/locate/gr

GR Letter

Stable carbon isotope chemostratigraphy of the base of the Callovian in Greenland

Ricardo L. Silva [a,*], Peter Alsen [b]

[a] Department of Earth Sciences and BETY Lab, Clayton H. Riddell Faculty of Environment, Earth, and Resources, University of Manitoba, 125 Dysart Road, Winnipeg, Manitoba R3T 2N2, Canada
[b] The Geological Survey of Denmark and Greenland, Øster Voldgade 10, DK-1350 Copenhagen K, Denmark

ARTICLE INFO

Article history:
Received 18 May 2024
Revised 31 July 2024
Accepted 28 August 2024
Available online 31 August 2024
Handling Editor: A. Festa

Keywords:
Stable carbon isotopes
Callovian
Greenland
Global Boundary Stratotype Section and Point
Standard Auxiliary Boundary Stratotype

ABSTRACT

D'Orbigny named the Callovian stage after Kellaways in Wiltshire, UK, in the 1850 s. However, agreement on its boundaries and, more recently, on the position and location of the Global Boundary Stratotype Section and Point (GSSP) for the base of the Callovian has proven difficult for the last 170 years. This is mainly due to the lack of agreement on the appropriate index fossil and its regional and global correlations, as well as the location of the stratotype section. Stable carbon isotope chemostratigraphy and event stratigraphy are now essential tools for aiding in the definition of GSSPs. In this study, stable carbon isotopic analysis of 91 samples from east Greenland's Middle Jurassic shallow marine sandstones of the Pelion Formation (Store Koldewey and Hold with Hope) and correlative and well-dated offshore siltstones and mudstones of the Fossilbjerget Formation (Jameson Land) is used to discriminate several isotopic events previously observed in other European basins and propose the early Callovian ($\delta^{13}C_{TOC}$) positive carbon isotopic excursion as a secondary marker for defining the Callovian GSSP. The early Callovian ($\delta^{13}C_{TOC}$) positive carbon isotopic excursion is a fundamental tool for superregional correlation between candidate GSSPs and Standard Auxiliary Boundary Stratotypes. It can also help establish a chronological order (synchronous vs diachronous) of species occurrences between different locations.

1. Introduction

The Callovian stage was named after Kellaways in Wiltshire, UK, by D'Orbigny in 1849–1852. To formally define this stage and its Global Boundary Stratotype Section and Point (GSSP), J.H. Callomon established and directed the Callovian Working Group in 1983 (Mönnig, 2014). However, over the next four decades, an agreement on the index fossil and its regional and global linkages and the location of the stratotype section has proven difficult. In the latest Geologic Time Scale 2020, and in the absence of a GSSP, the base of the Callovian was placed at the base of *K. keppleri*/*B. bullatus* ammonite chronozone (ACZ, Fig. 1a) and within a normal polarity-dominated interval tentatively correlated with Chron M39n.3n and with a projected age of 165.3 Ma (with ~ 1 Myr uncertainty) (Hesselbo et al., 2020).

The main issue so far has been that no Callovian section has been put forward that complies with all the International Commission on Stratigraphy criteria for establishing a GSSP (Remane et al., 1996). In 1990, the Callovian Working Group ratified the Albstadt-Pfeffingen section in the Baden-Wurttemberg region of southwest Germany as the Callovian GSSP candidate, with the "golden spike" in the first appearance datum (FAD) of *Kepplerites keppleri* at the base of the *M. herveyi* ACZ (Mönnig, 2014; Mönnig and Dietl, 2017). However, concerns regarding the condensed nature of the succession and numerous hiatuses have prevented a formal submission to the International Subcommission on Jurassic Stratigraphy. The expanded sections from the Volga region in Russia (Kiselev and Rogov, 2007) and East Greenland (Callomon et al., 2015) have been considered Standard Auxiliary Boundary Stratotype (SABS cf. Head et al., 2023) candidates on account of their more expanded nature and abundance of ammonites (Mönnig, 2014) (Fig. 1a and 1b).

Stable carbon isotopes chemostratigraphy and event stratigraphy are essential tools for the definition of many, if not all, GSSPs. Stable carbon isotopic records determined in a multitude of substrates are helpful for superregional correlation between sections and can also help with establishing a chronological order (synchronous vs diachronous) of species occurrences between different locations (Weissert et al., 2008). In this study, based on the stable

* Corresponding author.
E-mail address: ricardo.silva@umanitoba.ca (R.L. Silva).

https://doi.org/10.1016/j.gr.2024.08.011
1342-937X/

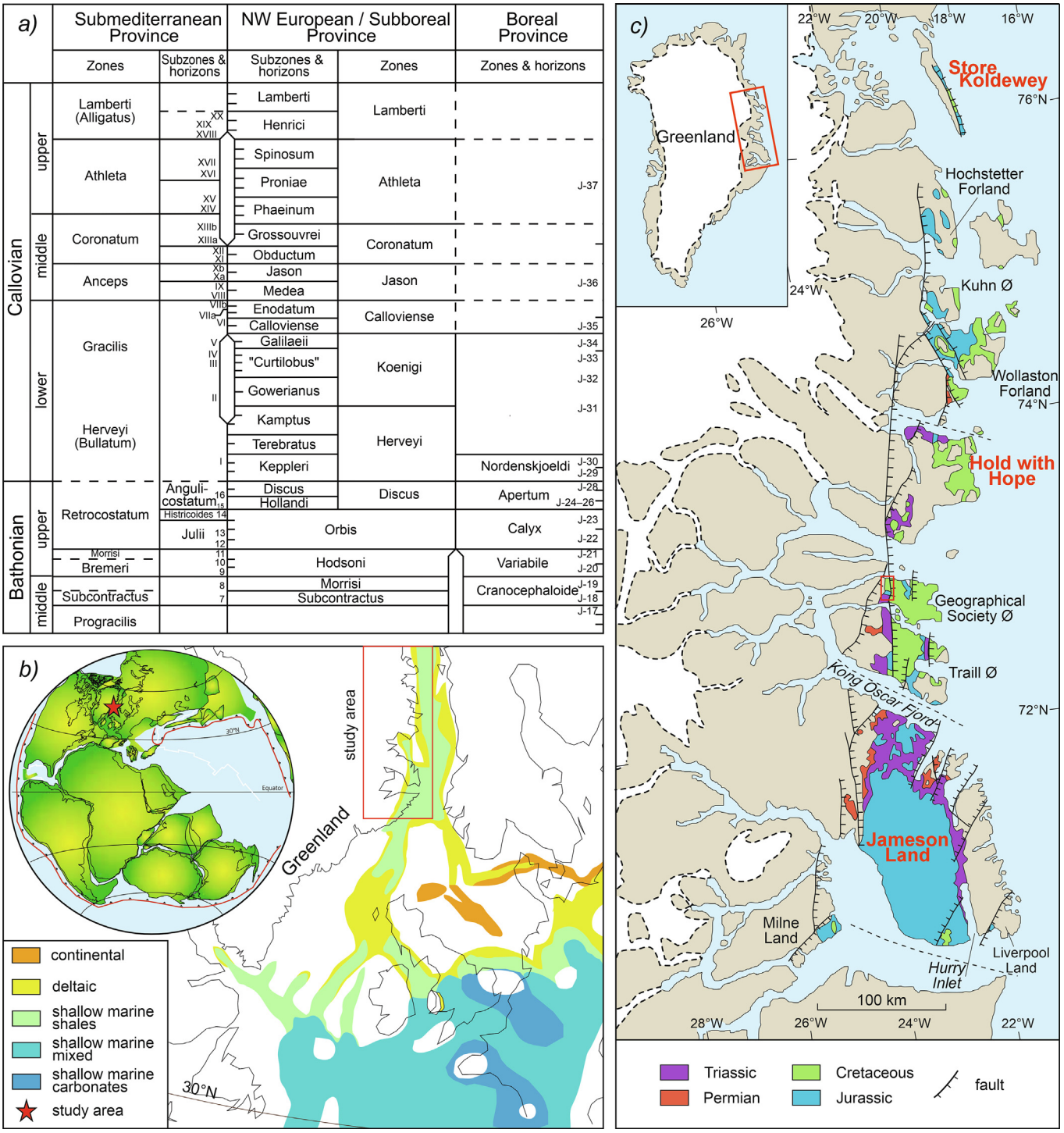

Fig. 1. (A) Ammonite correlation chart with the European and Boreal standard chronostratigraphy for the middle Bathonian–upper Callovian (Callomon et al., 2015). (B) Middle and Late Jurassic paleogeography of the Euro-Boreal region (Torsvik et al., 2002). (C) Simplified geological map of East Greenland with location of the study areas (Bojesen-Koefoed et al., 2023).

carbon isotopic analysis of 91 samples from the Middle Jurassic successions from Jameson Land (Fig, 1b), Hold with Hope, and Store Koldewey in East Greenland, we (1) update the $\delta^{13}C_{TOC}$ chemostratigraphy framework for the upper Bathonian–lowermost upper Callovian and (2) propose the early Callovian ($\delta^{13}C_{TOC}$) positive carbon isotopic excursion (CIE) (cf. Silva et al., 2020) as a secondary marker for the Callovian GSSP and a primary or secondary marker for the Callovian SABSs.

2. Geological background

Jurassic rocks are widely distributed in central East and North-East Greenland, occupying approximately 800 km of coast, from Jameson Land in the south to Store Koldewey in the north (Fig. 1b and 1c). The East Greenland basins formed the western-most segment of a major north–south oriented system of rift basins situated between Greenland and Norway (Fig. 1c)

(Engkilde and Surlyk, 2003). Deposition in the area during the Early Jurassic occurred under a period of relative tectonic quiescence, ensuing Late Permian–earliest Triassic and Early Triassic rift phases. This was followed by a long-term extensional phase in the Middle Jurassic (Late Bajocian), which peaked in the Late Jurassic (Kimmeridgian–Volgian) and waned in the earliest Cretaceous (Valanginian) (Surlyk, 2003, 1977). The Middle Jurassic of Greenland is a well-exposed example of the inshore to offshore successions characteristic of the rifted seaways in the Northwest European–North Atlantic region (Engkilde and Surlyk, 2003).

The upper Bajocian–middle Callovian early-rift succession of interest for this study comprises the offshore siltstones and mudstones of the Fossilbjerget Formation (Jameson Land, Supplementary Data, Fig. S1) and the correlative shallow marine sandstones of the Pelion Formation (Store Koldewey and Hold with Hope, Supplementary Data, Figs S2 and S3). Deposition was characterized by southwards progradation of the sediments now comprising the Pelion Formation in the late Bajocian, followed by major backstepping in Bathonian–Callovian, and drowning of the sandy depositional system in the middle-late Callovian (Alsen and Surlyk, 2004; Engkilde and Surlyk, 2003; Surlyk, 2003, 1977; Surlyk et al., 2021, 1973). The Jameson Land successions are rich in ammonites and allow for detailed bio- and chronostratigraphic correlation at local and superregional scales (e.g. (Callomon, 1993; Callomon et al., 2015; Mönnig and Dietl, 2017) (Fig. 1a).

2.1. A brief description of the study sections

2.1.1. Fossilbjerget, Jameson Land

The Fossilbjerget section is located in the heart of Jameson Land, central Greenland (Fig. 1c). The type section of the Fossilbjerget Formation is defined here, framed by the Pelion Formation at the base and the Olympen Formation at the top (Surlyk et al., 2021). In the studied section, the Fossilbjerget Formation consists of approximately 100 m of silty, micaceous mudstones with subordinate fine-grained sandstone horizons (Supplementary Data, Fig. S1). Sandy horizons, sometimes glauconitic, are more prominent at the base of the section. Phosphatic nodules and sandy/calcareous concretions are also present. Several levels are rich in ammonites, belemnites, Brachiopods, bivalves, and *Thalassinoides* burrows, indicating an offshore marine depositional environment (Surlyk et al., 2021). The abundance of ammonites allows for ammonite biozonation at the horizon scale, indicating several minor hiatuses in a clearly cyclical sedimentary succession. The standard chronostratigraphy for this section is presented in Supplementary Data, Figure S1, and is discussed in detail in several studies (Alsen and Surlyk, 2004; Callomon, 1993; Surlyk et al., 2021, 1973). The boundary between the Upper Bathonian and Lower Callovian is placed around 13–20 m from the base of the Fossilbjerget Formation.

2.1.2. Steensby Bjerg, Hold with Hope

The Steensby Bjerg section is located on the north coast of the Hold with Hope area (Fig. 1c). The study interval is assigned to the lower sandstone unit and Spath Plateau Member of the Pelion Formation (Surlyk et al., 2021) (Supplementary Data, Fig. S2). The lower sandstone unit consists of sandstone with trough cross-bedding and pebble lags at their base. The Spath Plateau Member consists of several coarsening-upward sandy beds. Frequently, the base is silty and has planar and cross-lamination (lower shale unit). Upwards, each sequence becomes sandier with planar and trough cross-bedding. The contact with the framing lithostratigraphic units is erosive. The observed lithologies and diversity and abundance of dinoflagellates suggest that deposition occurred in tidally influenced deltas with distributary channels and mouth bars in the lower–middle shoreface (Piasecki et al., 2004b; Surlyk et al., 2021).

This section and its standard chronostratigraphy presented in Supplementary Data, Figure S2, are discussed in detail in several publications (Callomon, 1993; Piasecki et al., 2004b; Surlyk et al., 2021; Vosgerau et al., 2004). Ammonites are rare in the study interval, with *P. koenigi* being identified at the top of the lower sandstone unit (Callomon, 1993). Dinoflagellate chronostratigraphy indicates a Lower–Upper Callovian age, equivalent to the *C. apertum–P. athleta* ammonite chronozones (Piasecki et al., 2004b; Surlyk et al., 2021).

2.1.3. Ravn Pynt, Store Koldewey

The Ravn Pynt section is located on Store Koldewey Island (Fig. 1c). The study interval corresponds to the Pelion Formation (Surlyk et al., 2021) (Supplementary Data, Fig. S3). The base of the section is predominantly fine-grained sandy, although with ammonites, belemnites, bivalves, and bioturbation. At around 17 m, the succession becomes more mud-rich, with rare ammonites at the base. The succession becomes sandier again at around 30 m and with planar cross-stratification. Ammonites, belemnites, oysters, fossil wood, and bioturbation, are common throughout this interval. Deposition occurred in tidally influenced deltas with distributary channels and mouth bars in the lower–middle shoreface (Piasecki et al., 2004a; Surlyk et al., 2021).

This section and the standard ammonite chronostratigraphy presented in Supplementary Data, Figure S3, are discussed in detail in (Piasecki et al., 2004a). These authors date this succession from the mid-Bathonian to Callovian based on ammonites and dinoflagellate cysts. Although a possible depositional break between the Bathonian and the Callovian parts of the Pelion Formation was suggested (Piasecki et al., 2004a), field campaigns by P. Alsen and J. Hovikoski in 2010 and 2014 recovered several ammonites from the base of the Spath Plateau Member, indicating that no major hiatus is discernible at this location around the Bathonian–Callovian boundary.

3. Materials and methods

Rock samples were sourced from the Geological Survey of Denmark and Greenland (GEUS) sample archive and sent to the University of Manitoba (Canada) for processing and analysis. All samples are referred to GEUS archive number and stratigraphic position (Supplementary Data, Table S1). The analyzed samples were collected during several fieldwork campaigns in East and North-East Greenland between 1974 and 2014.

Analysis of carbon % of the decarbonated fraction ($C_{decarbonated}$ %) and $\delta^{13}C_{TOC}$ (‰) was performed on 91 samples from Fossilbjerget (37 samples), Ravn Pynt, Store Koldewey (15 samples), and Hold with Hope (39 samples) section using an Eltra Helios Carbon Analyzer ($C_{decarbonated}$ %) and a Thermo Scientific Delta V Isotope Ratio Mass Spectrometer (IRMS) coupled with a Costech Elemental Combustion System-ECS 4010 ($\delta^{13}C_{TOC}$ ‰) at the Stable Isotope Laboratory (Manitoba Isotope Research Facility) of the University of Manitoba, Canada (Table S1). Before analysis, about 2–3 g of each powdered sample was decarbonated with ~ 40 ml HCl (1 M) in a water bath at 80 °C for two hours to ensure the complete reaction of all carbonate species. After allowing the reaction to continue for at least 24 h, the residue was rinsed three times (centrifuged) with deionized water until reaching neutral *pH* and dried at 35 °C. After drying, all decarbonated samples were first analyzed for carbon % of the decarbonated fraction using the Eltra Helios Carbon Analyzer (Supplementary Data). This was done to determine the amount of sample needed to ensure good linearity and signal intensity for the stable carbon isotopic analyses. After

$C_{decarbonated}$ % determination, the appropriate amount of decarbonated sample was weighed into 8 × 5 mm tin capsules for $\delta^{13}C_{TOC}$ analyses. Tin capsules containing decarbonated sample aliquots or the two standards, B2151 (sediment) and B2153 (soil) from Elemental Microanalysis, were loaded into an auto-sampler on the Costech Elemental Combustion System and combusted in an oxygen-rich environment. Calibration was performed by analyzing two international standards (USGS40, USGS41) at the beginning, middle and end of each run. A calibration line was calculated by least squares linear regression using the known and measured isotope values of the calibration standards. Replicate analyses of the two QC standards yielded the results of $\delta^{13}C_{VPDB}$=-26.34 ± 0.17 ‰ (n = 10) for B2151 and $\delta^{13}C_{VPDB}$=-26.94 ± 0.14 ‰ (n = 24) for B2153. Isotope ratios are reported in standard delta notation relative to Vienna PDB (Coplen, 1994).

4. Results

The carbon content of the decarbonated fraction ($C_{decarbonated}$ %) and determined $\delta^{13}C_{TOC}$ for each of the studied sections is presented in Supplementary Data, Table S1 and plotted in Figures S1, S2, and S3. The carbon content of the decarbonated fraction ($C_{decarbonated}$ %) from Fossilbjerget (Jameson Land, Supplementary Data, Fig. S1) ranges from 0.2 to 2.0 %, averaging around 0.6 %. The highest $C_{decarbonated}$ % was determined in the middle of the section. The determined $\delta^{13}C_{TOC}$ values range from −25.5 to −22.4 ‰. LOESS (locally estimated scatterplot smoothing) modelling indicates that a negative $\delta^{13}C_{TOC}$ characterizes the upper Bathonian succession. A sharp positive shift of about 1.5–2 ‰ is initiated at the base of the *C. apertum* ACZ (ammonite horizons J24-*C. apertum* α – J27-*K. tenuifasciculatus* and terminates in the *C nordenskjoeldi* ACZ (ammonite horizon J29 – *C. nordenskjoeldi* α and J30-*C. nordenskjoeldi* β (Callomon, 1993). The $\delta^{13}C_{TOC}$ record is relatively constant up the top of the studied part of the section, dated from the *S. calloviense* ACZ (ammonite horizons J34/35, *K. galilaeii*/*S. calloviense* (Callomon, 1993). There is no appreciable correlation between $C_{decarbonated}$ and $\delta^{13}C_{TOC}$ (r^2 = 0.22).

The carbon % of the decarbonated fraction ($C_{decarbonated}$ %) from Steensby Bjerg (Hold with Hope, Supplementary Data, Fig. S2) ranges from 0.004 to 8.8 %, averaging around 0.7 %. The highest $C_{decarbonated}$ % was determined in one sample from the top of the section. The determined $\delta^{13}C_{TOC}$ values range from −29.1 to −22.0 ‰ and LOESS modelling indicates that a negative $\delta^{13}C_{TOC}$ characterizes the lower Callovian part of the succession. The $\delta^{13}C_{TOC}$ trend is relatively stable in the lower and middle (*K. jason* ACZ) Callovian. A sharp positive shift of about 2–2.5 ‰ is observed in the mid-*P. athleta* ACZ. There is no appreciable correlation between $C_{decarbonated}$ and $\delta^{13}C_{TOC}$ (r^2 = 0.17).

$C_{decarbonated}$ % from the Ravn Pynt (Store Koldewey, Supplementary Data, Fig S3) section ranges from 0.1 to 2.1 %, averaging around 0.69 %. The highest $C_{decarbonated}$ % was determined in the middle of the section, dated as *S. koenigi* ACZ. The determined $\delta^{13}C_{TOC}$ values range from −24.9 to −23.0 ‰. LOESS modelling shows a sharp positive shift of about 1–1.5 ‰ initiated in the upper Bathonian, peaking in an undated interval. Afterwards, the $\delta^{13}C_{TOC}$ trend remains stable throughout the *S. koenigi* ACZ. There is no appreciable correlation between $C_{decarbonated}$ and $\delta^{13}C_{TOC}$ (r^2 = 0.16).

5. Discussion

5.1. Source of organic matter and meaning of the $\delta^{13}C_{TOC}$ record

Records of $\delta^{13}C_{TOC}$ often represent a mixed $\delta^{13}C$ signal from terrestrial and aquatic organisms, microbial biomass, and diagenesis, which can result in a highly variable $\delta^{13}C$ signature (Silva et al., 2020; Suan et al., 2015). The carbon isotopic composition of OM mainly depends on the carbon source, process of carbon assimilation (e.g., photosynthesis vs heterotrophy), metabolism, and cellular carbon budgets (e.g., Hoefs, 2015). Despite limitations, $\delta^{13}C_{TOC}$ profiles are useful for tracing changes in the global carbon cycle, thus, their widespread use in chemostratigraphic studies (Silva et al., 2021; Suan et al., 2015; Weissert et al., 2008).

One of the difficulties in interpreting $\delta^{13}C_{TOC}$ profiles is determining the carbon source. This is important because marine and terrestrial/continental carbon sources have different $\delta^{13}C$ values; therefore, changes in OM can lead to stratigraphic variation in $\delta^{13}C_{TOC}$ (Suan et al., 2015). Upper Bajocian–Bathonian fossil wood from Yorkshire (UK) presents an average $\delta^{13}C$ around –23 to –22 ‰ and ranges between −24.2 to −21.6 ‰ (Hesselbo et al., 2003). In the mid-Callovian Oxford Clay Formation (UK), eleven fossil wood samples have an average $\delta^{13}C$ of –23.8 ‰ (Kenig et al., 1994). These authors estimated an average $\delta^{13}C$ of –23.5 ‰ for terrestrial OM ($\delta^{13}C_{terrestrial}$) and between −29.1 to −26.6 ‰ for primary marine OM. The above-mentioned estimate for $\delta^{13}C_{marine}$ is corroborated by the $\delta^{13}C_{TOC}$ record from the marine upper Bathonian–lower Callovian from the Lusitanian Basin, ranging between −27.0 to −26.5 ‰. Based on the studies of Kenig et al. (1994) and Hesselbo et al. (2003), a $\delta^{13}C_{terrestrial}$ range between ~ -25 and –22 ‰ is assumed for the Bathonian–Callovian interval.

Palynological studies indicate that terrestrial woody material and palynomorphs dominate the kerogen assemblages of the Fossilbjerget Formation at Fossilbjerget and Spath Plateau Member of the Pelion Formation at Hold with Hope and Store Koldewey, despite the occurrence of minor amounts of dinoflagellate cysts (Piasecki et al., 2004b, 2004a; Smelror, 1988). The upper Bathonian–lower Callovian $\delta^{13}C_{TOC}$ from Greenland ranges between −25 and –22 ‰, averaging –23.7 ‰ at Fossilbjerget, −24.3 ‰ at Hold with Hope, and –23.8 ‰ at Store Koldewey (Table S1). The overall depositional environment of the study sections (Piasecki et al., 2004b, 2004a; Smelror, 1988; Surlyk et al., 2021) and the good correspondence between the Bathonian–Callovian range for $\delta^{13}C_{terrestrial}$ and the $\delta^{13}C_{TOC}$ record from the Greenland sections suggest that the kerogen assemblages of the studied samples are dominated by terrestrial organic matter. This indicates that the observed $\delta^{13}C_{TOC}$ trends are not related to major changes in the type of organic matter, i.e., marine vs terrestrial.

5.2. Stable carbon isotope chemostratigraphy of the upper Bathonian–middle Callovian

The regional carbonate $\delta^{13}C$ profile for the Bathonian–Callovian boundary includes the early–late Bathonian ($\delta^{13}C_{carb}$) negative CIE, late Bathonian–early Callovian ($\delta^{13}C_{carb}$) positive CIE, and the early Callovian ($\delta^{13}C_{carb}$) negative CIE (e.g., Bartolini et al., 1999; Jach et al., 2014; Jenkyns et al., 2002; Kenig et al., 1994; Koevoets et al., 2016; Nunn et al., 2009; O'Dogherty et al., 2006; Silva et al., 2020) (Fig. 2). In the well-dated La Cornicabra section of the External Subbetic Basin (Spain), the early–late Bathonian ($\delta^{13}C_{carb}$) negative CIE has an amplitude of about 0.5 ‰, the late Bathonian–early Callovian ($\delta^{13}C_{carb}$) positive CIE has an amplitude of ~ 0.8 ‰, and the early Callovian ($\delta^{13}C_{carb}$) negative CIE has an amplitude of about 0.9 ‰ (O'Dogherty et al., 2006) (Figs. 2 and 3). The record of $\delta^{13}C$ in organic matter for the lower Callovian is discussed below.

Stable carbon isotope datasets from total organic matter that cover the middle Callovian are scarce and usually have low temporal resolution (e.g., Kenig et al., 1994; Nunn et al., 2009; Jach et al., 2014; Koevoets et al., 2016) (Fig. 2). Kenig et al. (1994) presented a characterization of the Peterborough Member of the Oxford Clay Formation, uppermost lower Callovian (*S. calloviense* ACZ)–mid-

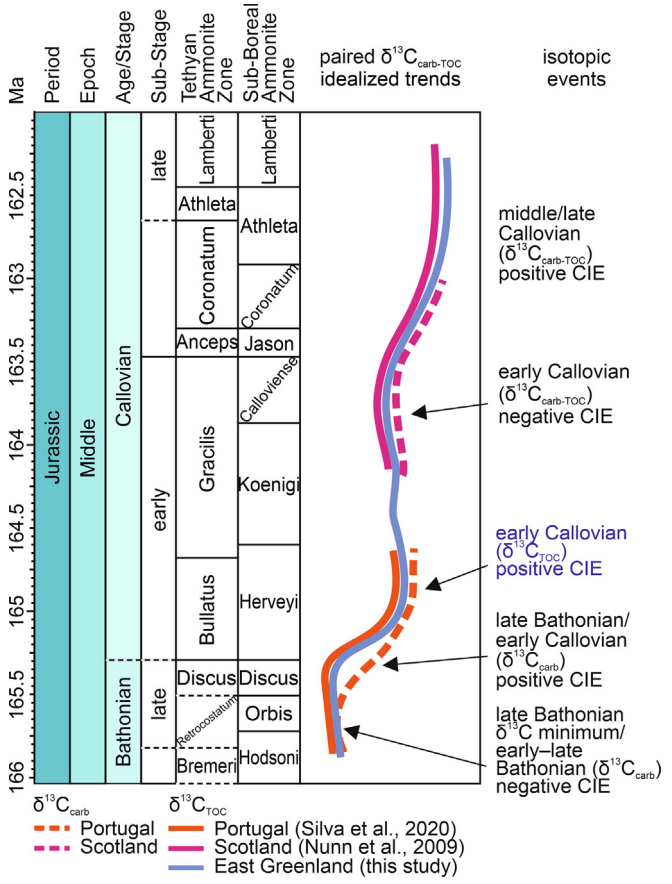

Fig. 2. Composite $\delta^{13}C$ curve for the middle Bathonian–Callovian (ages as in (Hesselbo et al., 2020), generated using TSCreator V8.0). Data from East Greenland is from this study (Fossilbjerget, Jameson Land, and Steensby Bjerg, Hold with Hope) Portugal is from (Silva et al., 2020) and Scotland is from (Nunn et al., 2009).

upper Callovian (*P. athleta* ACZ, *K. proniae* ammonite subchronozone, ASCZ). The lower Callovian $\delta^{13}C_{TOC}$ presents some variation, recording an overall negative trend in the *S. calloviense* ACZ (*S. calloviense* ASCZ). The interval between *S. calloviense* ACZ (*S. enodatum* ASCZ) and *K. jason* ACZ (*K. grossouvrei* ASCZ) (middle Callovian) has more stable $\delta^{13}C_{TOC}$ values. Except for one sample, $\delta^{13}C_{TOC}$ in this interval varies within ~ 1 ‰, between ~ -27.5 to ~ -26.5 ‰. A positive shift of similar amplitude is apparent from LOESS modelling of the $\delta^{13}C_{TOC}$ data from Hold with Hope (Fig. S2). Upwards, a positive shift of approximately 1.5 ‰ characterizes the transition between the *E. coronatum* ACZ (*K. grossouvrei* ASCZ) and *P. athleta* ACZ (*K. phaeinum*/*K. proniae* ASCZs). The top of the lower Callovian–middle Callovian was also analyzed at Staffin Bay, Isle of Skye, Scotland, at a relatively low resolution. Here, the interval dated from *P. koenigi* to *P. athleta* ACZs is characterized by a ~ 2 ‰ positive excursion, from −25 to −23 ‰ (Nunn et al., 2009). The middle–late Callovian ($\delta^{13}C_{carb-TOC}$) positive CIE is recorded in the upper part of the Hold with Hope section (Fig. 2 and S2).

Broadly, the Bajocian/Bathonian is interpreted as an interval of high eccentricity, high carbonate production, relatively low $\delta^{13}C$, and lower temperatures and annually dry climate interrupted by short periods of intensive rainfalls (Andrieu et al., 2016; Lécuyer et al., 2003; Martinez and Dera, 2015; Price, 1999). It was postulated that these conditions favoured the export of ^{12}C and carbonates from land to the oceans and promoted high evaporation, oceanic carbonate supersaturation, and oligotrophic conditions (Andrieu et al., 2016). The $\delta^{13}C_{carb-TOC}$ minimum during the Late Bathonian (Figs. 2 and 3) is interpreted to have resulted from the overall efficient oxidizing conditions in seawater and low carbon burial efficiency under oligotrophic conditions (Andrieu et al., 2016; Martinez and Dera, 2015) during a secular sea-level low (Haq et al., 1987). The recovery towards more positive $\delta^{13}C_{carb}$ values and decoupling of the paired $\delta^{13}C_{carb-TOC}$ with invariant $\delta^{13}C_{TOC}$ coincides with the onset of the transition to the Middle Callovian–Early Oxfordian paleoenvironmental mode. This time interval is characterized by low eccentricity, higher $\delta^{13}C$, low carbonate production, more eutrophic conditions, and humid and more seasonally contrasting climates (e.g. (Alberti et al., 2017; Andrieu et al., 2016; Lécuyer et al., 2003; Martinez and Dera, 2015; Price, 1999)).

In detail, Silva et al. (2020) suggested that the Early Callovian $\delta^{13}C_{TOC}$ positive CIE (and recoupling with $\delta^{13}C_{carb}$) resulted from increased export of oceanic organic carbon into sediments, materialized by lower Callovian black-shale and organic-rich intervals observable in Spain (*B. bullatus* ACZ, Lower Callovian, Gräfe, 2005), Northeast Scotland (*M. macrocephalus* ACZ, Lower Callovian, Nagy et al., 2001), central North America (Lower Callovian, Imlay, 1981), Himalayas (*C. discus*?–*P. gracilis* ACZs, Upper Bathonian–Lower Callovian, Yin, 2007), east Greenland (Lower Callovian, (Callomon, 1993), Atlantic Canada (Lower Callovian, Mukhopadhyay and Wade, 1990), west-Gulf of Mexico (Cantú–Chapa, 1969) and Japan (Handa et al., 2014; Kusuhashi et al., 2002). The apparent superregional and synchronous nature of the early Callovian ($\delta^{13}C_{TOC}$) positive CIE supports this interpretation. Increased organic carbon burial is also assumed as the cause of the middle–late Callovian ($\delta^{13}C_{carb-TOC}$) positive CIE. Organic-rich facies of Middle Callovian age are known from Southern England (*K. jason, E. coronatum*, and *P. athleta* ACZs Kenig et al., 1994), northeast Scotland (Calloviense and Jason zones, Lower-Middle Callovian, Nagy et al., 2001), Isle of Skye (*K. jason* and *E. coronatum*, Middle Callovian, Fisher and Hudson, 1987), and Belarus (*S. calloviense* ACZ, Lower Callovian, Makhnach and Tesakova, 2015).

5.3. The early Callovian ($\delta^{13}C_{TOC}$) positive CIE: An aid in the quest of the Callovian GSSP and SABSs

A detailed $\delta^{13}C_{TOC}$ curve for the Bathonian–Callovian boundary was published from Portugal (Silva et al., 2020) and allows for comparison with East Greenland (Fig. 3). In Portugal, a minimum in $\delta^{13}C_{carb-TOC}$ is recorded around the *H. julii*/*E. histricoides* ASCZs (*H. retrocostatum* ACZ), interpreted as the $\delta^{13}C$ minimum interval of the early–late Bathonian ($\delta^{13}C_{carb}$) negative CIE. The $\delta^{13}C_{carb-TOC}$ dataset is then characterized by decoupling the carbonate and TOC records, from the upper Bathonian (*H. retrocostatum* ACZ, *E. histricoides ASCZ*)–lower Callovian?. The termination of the decoupling event is materialized by the 1.5 ‰ amplitude early Callovian ($\delta^{13}C_{TOC}$) positive CIE, associated with the later stages of the late Bathonian–early Callovian ($\delta^{13}C_{carb}$) positive CIE.

In the Fossilbjerget section of Jameson Land, a positive CIE of about 1.5 ‰ initiates around ammonite horizons J24-J26, the base of the *C. apertum* ACZ, and is here interpreted as the early Callovian ($\delta^{13}C_{TOC}$) positive CIE (cf. (Silva et al., 2020). The early Callovian ($\delta^{13}C_{TOC}$) positive CIE extends until the *C. nordenskjoeldi* ACZ, terminating between ammonite horizons J30-J31?. Relatively stable $\delta^{13}C_{TOC}$ values characterize the interval just below J31? and J34-J35, signalling the end of the positive CIE. A slight negative trend of about 1 ‰ is observed in the *M. herveyi–S. koenigi* ACZ interval.

The East Greenland data shows that the early Callovian ($\delta^{13}C_{TOC}$) positive CIE spans the Bathonian–Callovian boundary. Despite the relatively low resolution of the dataset (a reflection of available samples from the GEUS archives), the positive CIE is constrained to the last zone of the Bathonian and the first zone of the Callovian. In conjunction with the Portuguese dataset, the only two datasets of good density and coverage, the early Callovian ($\delta^{13}C_{TOC}$) positive CIE (cf. (Silva et al., 2020) is here posited as a

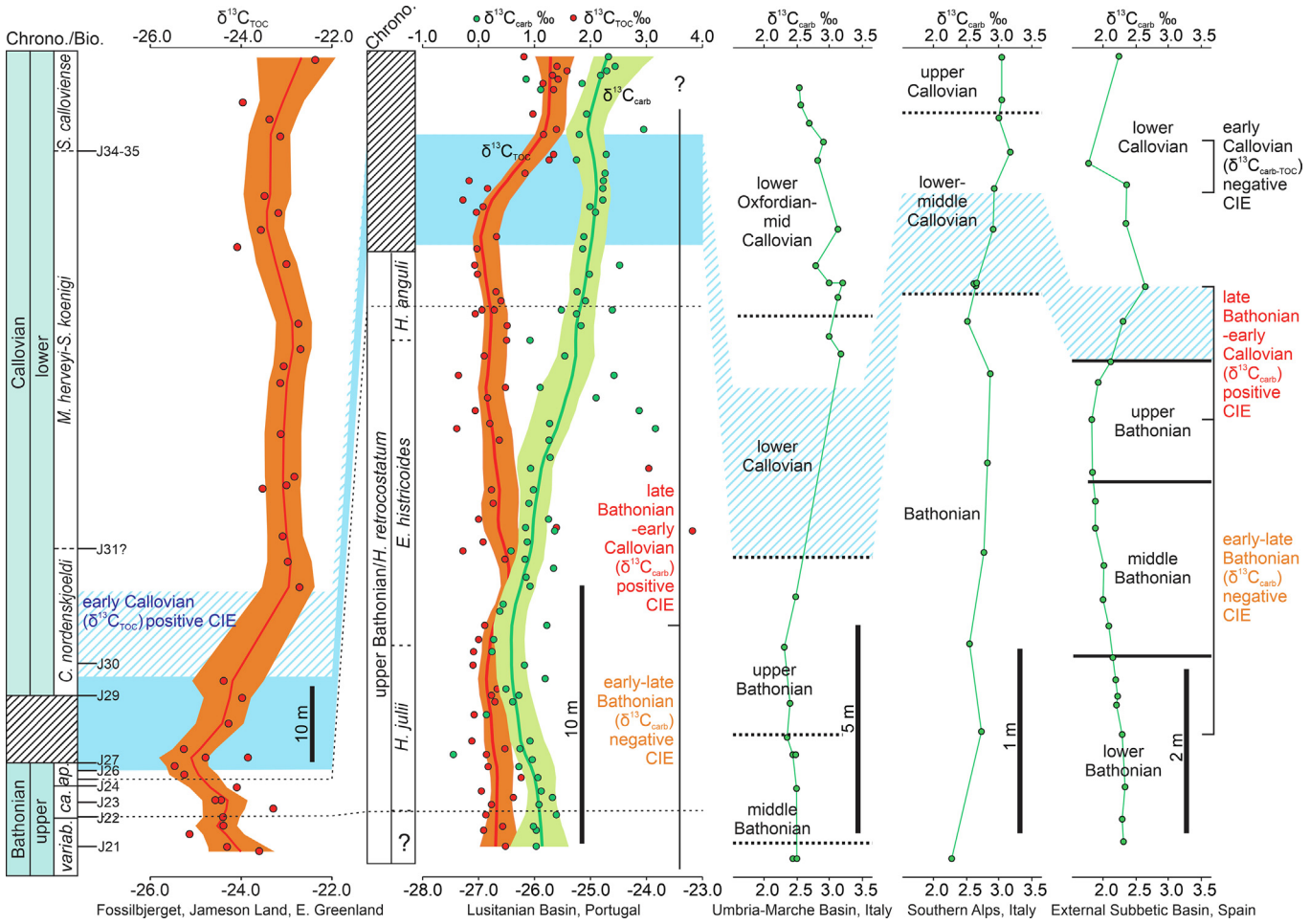

Fig. 3. $\delta^{13}C_{TOC}$ record of the middle Bathonian–lower Callovian in East Greenland, (chronostratigraphy according to (Callomon, 1993; Callomon et al., 2015) and comparison with the $\delta^{13}C$ record from the Lusitanian Basin (Silva et al., 2020), Umbria-Marche Basin (Bartolini et al., 1996); Southern Alpes (Jenkyns, 1996), External Subbetic Basin (O'Dogherty et al., 2006) (LOESS modelling was applied to the Greenland and Lusitanian Basin datasets, smoothing factor = 0.2, confidence interval = 95 %). The Fossilbjerget section is used here as it is the most complete section and has the most detailed bio- and chronostratigraphic framework of all three sections from Greenland.

marker for the Bathonian–Callovian transition, thus adding a new criterion (secondary marker cf. Murphy and Salvador, 1999) for the establishment of the Callovian GSSP. Because of the now apparent superregional and synchronous nature of the early Callovian ($\delta^{13}C_{TOC}$) positive CIE, this event will contribute to the enlightenment of superregional faunal relationships between different geographic domains, and candidate GSSP and SABSs (Fig. 1A and 1B). The lack of accessibility would, *a priori*, refrain any Greenland section from being a candidate for the Callovian GSSP. However, since requirements for SABSs follow ICS guidelines for GSSPs but can be applied with greater flexibility (Head et al., 2023), the (i) expanded and continuous sedimentary record, (ii) recognition of the early Callovian $\delta^{13}C_{TOC}$ positive CIE, and (iii) paleontological richness makes the Fossilbjerget section a candidate for the Callovian SABS for the Boreal Province.

6. Conclusions

We analyzed 91 samples from east Greenland's middle Jurassic shallow marine sandstones of the Pelion Formation (Store Koldewey and Hold with Hope) and correlative offshore siltstones and mudstones of the Fossilbjerget Formation (Jameson Land). The obtained data allowed us to discriminate several isotopic events. We recognize the early Callovian ($\delta^{13}C_{TOC}$) positive CIE as a superregional isotopic event that straddles the Batonian–Callovian boundary, thus adding an important chemostratigraphy marker for the establishment of the elusive Callovian GSSP and its SABSs.

Funding

This work was supported by the Natural Sciences and Engineering Research Council of Canada via a Discovery Grant [grant number RGPIN-2024–04888].

CRediT authorship contribution statement

Ricardo L. Silva: Writing – review & editing, Writing – original draft, Visualization, Supervision, Project administration, Methodology, Investigation, Funding acquisition, Formal analysis, Data curation, Conceptualization. **Peter Alsen:** Writing – review & editing, Resources, Project administration, Conceptualization.

Data availability

Data will be made available on request.

Declaration of competing interest

The authors declare that they have no known competing financial interests or personal relationships that could have appeared to influence the work reported in this paper.

Acknowledgments

Samples were kindly provided partly from the GEUS archive and collected by numerous colleagues, e.g. T. Birkelund, C. Heinberg, H. Vosgerau, J. Therkelsen, M. Larsen, L. Stemmerik, and S. Piasecki. We want to express our gratitude to the editor, Andrea Festa, and the two reviewers for their valuable feedback, which significantly enhanced this manuscript. Natural Sciences and Engineering Research Council of Canada supports R. Silva via a Discovery Grant (grant number RGPIN-2024-04888).

Appendix A. Supplementary data

Supplementary data to this article can be found online at https://doi.org/10.1016/j.gr.2024.08.011.

References

Alberti, M., Fürsich, F.T., Abdelhady, A.A., Andersen, N., 2017. Middle to Late Jurassic equatorial seawater temperatures and latitudinal temperature gradients based on stable isotopes of brachiopods and oysters from Gebel Maghara. Egypt. Palaeogeogr. Palaeoclimatol. Palaeoecol. 468, 301–313. https://doi.org/10.1016/j.palaeo.2016.11.052.

Alsen, P., Surlyk, F., 2004. Maximum Middle Jurassic transgression in East Greenland: evidence from new ammonite finds, Bjørnedal. Traill ø. GEUS Bull. 5, 31–49. https://doi.org/10.34194/geusb.v5.4806.

Andrieu, S., Brigaud, B., Barbarand, J., Lasseur, E., Saucède, T., 2016. Disentangling the control of tectonics, eustasy, trophic conditions and climate on shallow-marine carbonate production during the Aalenian-Oxfordian interval: from the western France platform to the western Tethyan domain. Sediment. Geol. 345, 54–84. https://doi.org/10.1016/j.sedgeo.2016.09.005.

Bartolini, A., Baumgartner, P.O., Hunziker, J., 1996. Middle and Late Jurassic carbon stable-isotope stratigraphy and radiolarite sedimentation of the Umbria-Marche basin (central Italy). Eclogae Geol. Helv. 89, 811–844. https://doi.org/10.5169/seals-167925.

Bartolini, A., Baumgartner, P.O., Guex, J., 1999. Middle and Late Jurassic radiolarian palaeoecology versus carbon-isotope stratigraphy. Palaeogeogr. Palaeoclimatol. Palaeoecol. 145, 43–60. https://doi.org/10.1016/S0031-0182(98)00097-2.

Bojesen-Koefoed, J.A., Alsen, P., Bjerager, M., Hovikoski, J., Ineson, J.R., Johannessen, P.N., Olivarius, M., Piasecki, S., Vosgerau, H., 2023. The Rødryggen-1 and Brorson Halvø-1 fully cored boreholes (Upper Jurassic – Lower Cretaceous), Wollaston Forland, North-East Greenland – an introduction. GEUS Bull. 55. https://doi.org/10.34194/geusb.v55.8350.

Callomon, J.H., 1993. The ammonite succession in the Middle Jurassic of East Greenland. GEUS Bull. 40, 83–113.

Callomon, J.H., Alsen, P., Surlyk, F., 2015. The ammonites of the Middle Jurassic Cranocephalites beds of East Greenland. GEUS Bull. 34, 1–86. https://doi.org/10.34194/geusb.v34.4488.

Cantú-Chapa, A., 1969. Estratigrafía del Jurásico Medio-Superior del subsuelo de Poza Rica, Ver. (Área de Soledad–Miquetla). Revista Del Instituto Mexicano Del Petróleo 1, 3–9.

Coplen, T.B., 1994. Reporting of stable hydrogen, carbon, and oxygen isotopic abundances (Technical Report). Pure Appl. Chem. 66, 273–276. https://doi.org/10.1351/pac199466020273.

Engkilde, M., Surlyk, F., 2003. Shallow marine syn-rift sedimentation: Middle Jurassic Pelion Formation, Jameson Land. East Greenland. GEUS Bull. 1, 813–863. https://doi.org/10.34194/geusb.v1.4690.

Fisher, I., St, J., Hudson, J.D., 1987. Pyrite formation in Jurassic shales of contrasting biofacies. Geol. Soc. Spec. Publ. 26, 69–78. https://doi.org/10.1144/GSL.SP.1987.026.01.04.

Gräfe, K.-U., 2005. Benthic foraminifers and palaeoenvironment in the Lower and Middle Jurassic of the Western Basque-Cantabrian Basin (Northern Spain). J. Iber. Geol. 31, 217–233.

Handa, N., Nakada, K., Anso, J., Matsuoka, A., 2014. Bathonian/callovian (Middle Jurassic) ammonite biostratigraphy of the kaizara formation of the tetori group in central Japan. Newsl. Stratigr. 47, 283–297. https://doi.org/10.1127/0078-0421/2014/0048.

Haq, B.U., Hardenbol, J., Vail, P.R., 1987. Chronology of fluctuating sea levels since the triassic. Science 1979 (235), 1156–1167. https://doi.org/10.1126/science.235.4793.1156.

Head, M.J., Aubry, M.-P., Piller, W.E., Walker, M., 2023. Standard auxiliary boundary stratotype (SABS) approved to support the global boundary stratotype section and point (GSSP). Episodes 46, 99–100. https://doi.org/10.18814/epiiugs/2022/022044.

Hesselbo, S.P., Ogg, J.G., Ruhl, M., Hinnov, L.A., Huang, C.J., 2020. The Jurassic Period, in: Gradstein, F.M., Ogg, James G., Schmitz, M.D., Ogg, G.M. (Eds.), Geologic Time Scale 2020, Vol 2. Elsevier, pp. 955–1021. doi: 10.1016/B978-0-12-824360-2.00026-7.

Hesselbo, S.P., Morgans-Bell, H.S., McElwain, J.C., Rees, P.M., Robinson, S.A., Ross, C. E., 2003. Carbon-cycle perturbation in the middle jurassic and accompanying changes in the terrestrial paleoenvironment. J. Geol. 111, 259–276. https://doi.org/10.1086/373968.

Hoefs, J., 2015. Stable Isotope Geochemistry. Springer International Publishing. https://doi.org/10.1007/978-3-319-19716-6.

Imlay, R.W., 1981. Jurassic (Bathonian and Callovian) Ammonites in Eastern Oregon and Western Idaho. Geological Survey professional paper. U.S. Dept. of the Interior, Geological Survey, Washington, D.C..

Jach, R., Djerić, N., Goričan, Š., Reháková, D., 2014. Integrated Stratigraphy of The Middle-Upper Jurassic of the Krížna Nappe, Tatra Mountains. Ann. Soc. Geol. Pol. 84, 1–33.

Jenkyns, H.C., 1996. Relative sea-level change and carbon isotopes: data from the Upper Jurassic (Oxfordian) of central and Southern Europe. Terra Nova 8, 75–85. https://doi.org/10.1111/j.1365-3121.1996.tb00727.x.

Jenkyns, H.C., Jones, C., Gröcke, D., Hesselbo, S., Parkinson, D., 2002. Chemostratigraphy of the Jurassic System: applications, limitations and implications for palaeoceanography. J. Geol. Soc. London. 159, 351–378. https://doi.org/10.1144/0016-764901-130.

Kenig, F.G., Hayes, J.M., Popp, B.N., Summons, R.E., 1994. Isotopic biogeochemistry of the Oxford Clay Formation (Jurassic). UK. J. Geol. Soc. London. 151, 139–152. https://doi.org/10.1144/gsjgs.151.1.0139.

Kiselev, D.N., Rogov, M.A., 2007. Stratigraphy of the Bathonian-Callovian boundary deposits in the Prosek section (Middle Volga Region). Article 1. Ammonites and infrazonal biostratigraphy. Stratigr. Geol. Correl. 15, 485–515. https://doi.org/10.1134/S0869593807050036.

Koevoets, M.J., Abay, T.B., Hammer, Ø., Olaussen, S., 2016. High-resolution organic carbon–isotope stratigraphy of the Middle Jurassic-Lower Cretaceous Agardhfjellet Formation of central Spitsbergen. Svalbard. Palaeogeogr. Palaeoclimatol. Palaeoecol. 449, 266–274. https://doi.org/10.1016/j.palaeo.2016.02.029.

Kusuhashi, N., Matsuoka, H., Kamiya, H., Setoguchi, T., 2002. Stratigraphy of the late Mesozoic Tetori Group in the Hakusan Region, central Japan : an overview. Memoirs of the Faculty of Science. Kyoto University. Series Geol. and Min. 59, 9–31.

Lécuyer, C., Picard, S., Garcia, J.-P., Sheppard, S.M.F., Grandjean, P., Dromart, G., 2003. Thermal evolution of Tethyan surface waters during the middle-late jurassic: evidence from δ18O values of marine fish teeth. Paleoceanography 18, 1076. https://doi.org/10.1029/2002PA000863.

Makhnach, V.V., Tesakova, E.M., 2015. Palaeogeographic reconstructions of the natural environment in southeast Belarus during the Bathonian-Oxfordian ages. Moscow Univ. Geol. Bull. 70, 159–170. https://doi.org/10.3103/S0145875215020064.

Martinez, M., Dera, G., 2015. Orbital pacing of carbon fluxes by a ∼9-My eccentricity cycle during the Mesozoic. Proc. Natl. Acad. Sci. USA 112, 12604–12609. https://doi.org/10.1073/pnas.1419946112.

Mönnig, E., Dietl, G., 2017. The systematics of the ammonite genus Kepplerites (upper Bathonian and basal Callovian, Middle Jurassic) and the proposed basal boundary stratotype (GSSP) of the Callovian Stage. Neues Jahrb. Geol. Palaontol. Abh. 286, 235–287. https://doi.org/10.1127/njgpa/2017/0697.

Mönnig, E., 2014. Report of the Callovian Stage Task Group, 2013. Vol. Jurass. 12, 197–200.

Mukhopadhyay, P.K., Wade, J.A., 1990. Organic facies and maturation of sediments from three Scotian Shelf wells. Bull. Canadian Petrol. Geol. 38, 407–425.

Murphy, M.A., Salvador, A., 1999. International Stratigraphic Guide — An abridged version. Episodes 22, 255–271.

Nagy, J., Finstad, E.K., Dypvik, H., Merethe, A., Bremer, G.A., Bremer, M.G.A., 2001. Response of foraminiferal facies to Transgressive-Regressive cycles in the Callovian of northeast Scotland. J. Foraminiferal Res. 31, 324–349. https://doi.org/10.2113/0310324.

Nunn, E.V., Price, G.D., Hart, M.B., Page, K.N., Leng, M.J., 2009. Isotopic signals from Callovian-Kimmeridgian (Middle–Upper Jurassic) belemnites and bulk organic carbon, Staffin Bay, Isle of Skye. Scotland. J. Geol. Soc. London 166, 633. https://doi.org/10.1144/0016-76492008-067.

O'Dogherty, L., Sandoval, J., Bartolini, A., Bruchez, S., Bill, M., Guex, J., 2006. Carbon–isotope stratigraphy and ammonite faunal turnover for the Middle Jurassic in the Southern Iberian palaeomargin. Palaeogeogr. Palaeoclimatol. Palaeoecol. 239, 311–333. https://doi.org/10.1016/j.palaeo.2006.01.018.

Piasecki, S., Callomon, J.H., Stemmerik, L., 2004a. Jurassic dinoflagellate cyst stratigraphy of Store Koldewey. North-East Greenland. GEUS Bull. 5, 99–112. https://doi.org/10.34194/geusb.v5.4810.

Piasecki, S., Larsen, M., Therkelsen, J., Vosgerau, H., 2004b. Jurassic dinoflagellate cyst stratigraphy of Hold with Hope, North-East Greenland. GEUS Bull 5, 73–88. https://doi.org/10.34194/geusb.v5.4808.

Price, G.D., 1999. The evidence and implications of polar ice during the Mesozoic. Earth. Sci. Rev. 48, 183–210. https://doi.org/10.1016/S0012-8252(99)00048-3.

Remane, J., Bassett, M.G., Cowie, J.W., Gohrbandt, K.H., Lane, H.R., Michelsen, O., Naiwen, W., 1996. Revised guidelines for the establishment of global

chronostratigraphic standards by the International Commission on Stratigraphy (ICS). Episodes 19, 77–81. https://doi.org/10.18814/epiiugs/1996/v19i3/007.
Silva, R.L., Duarte, L.V., Wach, G.D., Morrison, N., Campbell, T., 2020. Oceanic organic carbon as a possible first-order control on the carbon cycle during the Bathonian-Callovian. Glob. Planet. Change. 184, 103058. https://doi.org/10.1016/j.gloplacha.2019.103058.
Silva, R.L., Duarte, L.V., Wach, G.D., Ruhl, M., Sadki, D., Gómez, J.J., Hesselbo, S.P., Xu, W., O'Connor, D., Rodrigues, B., Filho, J.G.M., 2021. An early jurassic (Sinemurian–Toarcian) stratigraphic framework for the occurrence of organic matter preservation intervals (OMPIs). Earth. Sci. Rev. 221, 103780. https://doi.org/10.1016/j.earscirev.2021.103780.
Smelror, M., 1988. Late Bathonian to Early Oxfordian dinoflagellate cyst stratigraphy of Jameson Land and Milne Land, East Greenland. Rapp. Grønl. Geol. Unders. 137, 135–159. https://doi.org/10.34194/rapggu.v137.8019.
Suan, G., van de Schootbrugge, B., Adatte, T., Fiebig, J., Oschmann, W., 2015. Calibrating the magnitude of the Toarcian carbon cycle perturbation. Paleoceanography 30, 495–509. https://doi.org/10.1002/2014PA002758.
Surlyk, F., 1977. Stratigraphy, tectonics and palaeogeography of the Jurassic sediments of the areas north of Kong Oscars Fjord, East Greenland. Bull. Georg. Acad. Sciencesetin Grønlands Geologiske Undersøgelse 123, 1–56. https://doi.org/10.34194/bullggu.v123.6665.
Surlyk, F., 2003. The Jurassic of East Greenland: a sedimentary record of thermal subsidence, onset and culmination of rifting. GEUS Bull. 1, 657–722. https://doi.org/10.34194/geusb.v1.4674.
Surlyk, F., Callomon, J.H., Bromley, R.G., Birkelund, T., 1973. Stratigraphy of the Jurassic – Lower Cretaceous sediments of Jameson Land and Scoresby Land, East Greenland. Bull. Grønl. Geol. Unders. 105, 1–76.
Surlyk, F., Alsen, P., Bjerager, M., Dam, G., Engkilde, M., Hansen, C.F., Larsen, M., Noe-Nygaard, N., Piasecki, S., Therkelsen, J., Vosgerau, H., 2021. Jurassic stratigraphy of East Greenland. GEUS Bull. 46. https://doi.org/10.34194/geusb.v46.6521.
Torsvik, T.H., Carlos, D., Mosar, J., Cocks, L.R.M., Malme, T.N., 2002. Global reconstructions and North Atlantic paleogeography 440 Ma to Recent. In: Eide, E.A. (Ed.), BATLAS mid Norway Plate Reconstruction Atlas with Global and Atlantic Perspectives. Geological Survey of Norway, Trondheim, pp. 18–39.
Vosgerau, H., Larsen, M., Piasecki, S., Therkelsen, J., 2004. A new Middle-Upper Jurassic succession on Hold with Hope. North-East Greenland. GEUS Bull. 5, 51–71. https://doi.org/10.34194/geusb.v5.4807.
Weissert, H., Joachimski, M., Sarnthein, M., 2008. Chemostratigraphy. Newsl. Stratigr. 42, 145–179. https://doi.org/10.1127/0078-0421/2008/0042-0145.
Yin, J., 2007. A review on Jurassic sea-level changes in Himalayan Tibet. Beringeria 37, 253–266.